J Solid State Eletrochem (2004) 8: 159–166
DOI 10.1007/s10008-003-0428-2

ORIGINAL PAPER

Antonello Vicenzo · Michela Rea · Luca Vonella
Massimiliano Bestetti · Pietro Luigi Cavallotti

Electrochemical deposition and structural characterization of Au-Sn alloys

Received: 28 November 2002 / Accepted: 10 March 2003 / Published online: 6 September 2003
© Springer-Verlag 2003

Abstract In the present work the electrochemical deposition of Au-Sn alloys is addressed and a cyanide-free process is presented. The electrolyte is an acidic thiourea solution containing gold as a $Au[CS(NH_2)_2]^+$ complex and tin as stannous ions. Results concerning the plating process development and deposit characterization are reported. Au-Sn alloy films with a Sn content up to 50 at% and a single-phase structure can be obtained from the acidic thiourea–Au(I) solution under pulsed current plating conditions. Alloy deposits show three main crystal structures: a face centred cubic (fcc) Au(Sn) solid solution, extending up to 7 at% Sn; a hexagonal close-packed structure, of the same type as the metallurgical ζ phase, up to about 18 at% Sn; and a NiAs-type structure, corresponding to the δ phase of the equilibrium diagram, with an enlarged homogeneity range. Mechanical properties of thin layers of Au-Sn alloys derived from micro-indentation measurements follow the structural modification with the alloy composition. The ordered intermetallic phases occurring in the equilibrium binary system, in particular the β and ζ' phases at 8 at% and 16 at% Sn, respectively, are not detected in the electrodeposited alloys. The main factors controlling electrochemical phase formation are pointed out, considering the differences between the phase structure of the electrodeposited alloys and the equilibrium phase diagram.

Presented at the 3rd International Symposium on Electrochemical Processing of Tailored Materials held at the 53rd Annual Meeting of the International Society of Electrochemistry, 15–20 September 2002, Düsseldorf, Germany

A. Vicenzo · M. Rea · L. Vonella · M. Bestetti
P. L. Cavallotti (✉)
Dipartimento di Chimica,
Materiali e Ingegneria Chimica "Giulio Natta",
Politecnico di Milano, Via Mancinelli 7, 20131 Milan, Italy
E-mail: pietro.cavallotti@polimi.it
Tel.: +39-02-23993149
Fax: +39-02-23993180

Keywords Au-Sn electrodeposition · Electrodeposits structure · Thiourea · White gold

Introduction

Electrodeposited Au-Sn alloys are suitable materials for decorative and engineering applications, as a starting binary system for the development of ternary alloys suitable as white gold coatings for jewellery finishing, and as hard solder coatings for optoelectronic and semiconductor devices [1].

Interest in the electrodeposition of Au-Sn alloys was originally stimulated by the search for white gold alloys [2]. Alkaline cyanide baths were developed, which, however, did not prove to be suitable for practical purposes. A renewed interest in Au-Sn plating has developed during the last 10 years, following the increasing importance of Au-Sn bonding technology and in the framework of research projects aimed at replacing Ni in the jewellery industry. In the technical literature, besides a few patents on Au-Sn plating [3], alkaline [4] and acidic [5] plating baths derived from earlier cyanide formulations have been recently proposed for hollow jewellery electroforming, while neutral cyanide-free baths are under development for bonding layer deposition [6], owing to the chemical incompatibility between cyanide and the positive photoresist commonly used in the manufacture of microelectronic devices.

The eligible solution chemistry for gold alloy plating baths is generally restricted to the cyanide and sulfite gold complexes, with still important stability issues for sulfite baths. An alternative approach is provided by the use of the Au(I)–thiourea complex [7]. Thiourea (TU) forms with Au(I) a single mononuclear cationic complex according to the following dissolution–complexation reaction [8]:

$$Au + 2CS(NH_2)_2 \rightleftharpoons Au\left[CS(NH_2)_2\right]_2^+ + e^- \quad (1)$$

The stability of the Au(I)–TU complex is restricted to an acidic environment, depending also upon the concentration of the metal cation and ligand [9], because of the oxidative degradation of thiourea itself, leading ultimately to the formation of elemental sulfur and cyanamide at high pH values [10]. The first oxidation product of thiourea is formamidine disulfide (FDS), which can be formed under weak oxidation conditions, chemically or electrochemically, on different metal electrodes, silver [11], platinum [12], or copper [13], according to the half reaction:

$$2CS(NH_2)_2 \rightleftharpoons (H_2N)_2(HN)_2C_2S_2 + 2e^- + 2H^+ \qquad (2)$$

The standard potential of the redox couple TU/FDS is 0.43 V [14].

The main interest of researchers has concentrated upon the use of thiourea in Au ores processing, even though the possibility of Au plating from thiourea solution was already disclosed in the late 1960s [15]. Further investigations in the former USSR, as reported by Groenwald [16, 17] and later by Juarez and Dutra [18], were especially concerned with hydrometallurgy applications and the feasibility of electrowinning processes.

A reliable pure Au electrodeposition process from acidic thiourea solution was developed as a primary goal of the present project and will be presented elsewhere.

Experimental

The Au(I)–TU solution was prepared by adding in drops a dilute Au(I) alkaline sodium sulfite solution (Engelhard) to an acidic thiourea solution [0.5–1 M H_2SO_4, 1 M $CS(NH_2)_2$]. During preparation the solution was kept at 40 °C under gentle stirring. Solutions with a low Au(I) concentration, below about 0.04 M, are colourless and clear; at higher concentration, the solution is pale yellow and tends to separate a fine yellowish precipitate, which was identified by XRD analysis as elemental sulfur. All other chemicals used were of reagent grade, except thiourea (lab grade, 98.5%).

Au-Sn deposits were prepared from solutions containing 1 M H_2SO_4, 1 M $CS(NH_2)_2$, 0.01–0.025 M Au(I), up to 0.1 M Sn(II), 0.6–18 mM KI, and ascorbic acid, under both direct current (DC) and pulsed current (PC) conditions, at a current density in the range 5–50 mA cm^{-2} and at 40 °C. For PC plating the off-time was varied in the range 1–10 s and the on-time in the range 0.1–5 s. Substrates were obtained from a Si wafer coated with either Cr/Ni/Au or Ta/Au blanket metallization. The Au layer was 100 nm thick.

The deposition conditions were investigated by linear sweep voltammetry (LSV), cyclic polarization (CP), and electrodeposition tests. The electrochemical setup consisted of a model 273A EG&G Princeton Applied Research and an AMEL System 5000 potentiostat/galvanostat for voltammetric measurements and PC deposition, respectively. A rotating Pt disk electrode was used, with apparent cathodic area of 0.2 cm^2, changing the rotation speed ω in the range 300–5000 rpm. CP runs were performed by setting the lower potential at 0.1 V and the vertex potential at −0.6 V (SCE), with a scan rate of 0.02 V s^{-1}; in LSV experiments the potential was driven in the cathodic direction at a scan rate of 0.001 V s^{-1} from the open circuit potential to about −0.6 V. LSV and CP runs were performed either on the Pt electrode or after deposition of a thin Au layer (1.5 mA cm^{-2}, 5 min). The solutions used for electrochemical measurements were deaerated by argon bubbling for about 1 h before use and were kept at 40 °C during measurement. The counter electrode was either an Au or a Sn wire. The potential was measured against a saturated calomel electrode (SCE).

The phase structure of the deposits was determined by X-ray diffraction (XRD) with filtered Cu Kα radiation, using both the standard powder method and glancing angle X-ray diffraction. Kα1 diffraction lines were used for calculations of the lattice parameters, which were refined by a least-squares method.

Vickers microhardness (HV) and elastic modulus (E) data were obtained from penetration depth–load curves by means of a Fischerscope H100 microhardness measurement system. Measurements were carried out on the sample surfaces with a peak load of 10 mN, loading/unloading time of 20 s, and 5 s holding time at peak load.

The surface morphology was investigated by scanning electron microscopy (SEM). The composition of the deposits was determined by energy dispersion spectroscopy (EDS).

Results

Chemical stability

In the acidic thiourea electrolyte, tin must be added as a Sn(II) salt and, since stannous ions can be easily oxidized to stannic ions by dissolved oxygen and other oxidizing agents, the chemical stability of the solution is an important issue in the development of the Au-Sn electroplating process. The standard potential of the redox couple Sn(II)/Sn(IV) is 0.151 V [19], which must be compared with the standard potential, 0.38 V [17], for gold discharge from $Au(TU)_2^+$ and the standard potential of the redox couple TU/FDS, 0.43 V. Therefore, Sn(II) ions could reduce the Au(I) complex and, in fact, the chemical stability of the solution is poor at low thiourea concentrations. FDS and other thiourea oxidation products, coming from chemicals as impurities or resulting from the preparation procedure, could also be oxidizing agents for Sn(II). However, according to our observations, these potential threats are not the primary factor responsible for electrolyte degradation. In fact, the solution prepared by adding tin(II) sulfate to the acidic Au(I)–TU electrolyte shows a relatively good stability on standing, which can be for several weeks. On the other hand, the kinetics of electrolyte degradation becomes accelerated when the solution is used for plating and this is probably related to the use of a Au-soluble anode, whose working potential, in the range of 0.1–0.15 V vs. SCE, is significantly above the oxidation potential of Sn(II) ions. The operating life of the plating bath was in general in the range from 7 to 10 days, the current fed to the cell being about 3 A h dm^{-3}, after which the solution turned cloudy, because of the formation of colloidal Sn(IV) hydroxide, which rapidly separated as a fine precipitate. Different reducing agents were tested as possible stabilizing additives, including pyrocatechol, ascorbic acid, citric acid, dextrin, and others, with modest improvement of electrolyte stability. Most of the reducing agents tested in the screening, even though more or less effective in preventing stannous ions oxidation, also have the drawback of being potential reducing agents for the Au(I)–TU complex. At the

current stage of electrolyte development, ascorbic acid has been found to be a suitable stabilizer and the results presented in the following refer to plating baths containing ascorbic acid in the concentration range 1–2 g L^{-1}. The Sn(II) concentration was also critical for the stability of the electrolyte and it was therefore fixed to a minimum value of 0.05 M, which, at least under PC plating conditions, enables the electrodeposition of Au-Sn alloys in the composition range of practical interest (i.e. from about 15 to 30 at%).

Electrochemical behaviour

LSV curves at an Au-plated Pt RDE in 1 M H_2SO_4, 1 M TU, and 0.025 M Au(I) solution at 40 °C, and varying potential scan rates, are shown in Fig. 1. The shape of the curves indicates that the discharge of the Au(I)–TU complex, which takes place in the potential range around −0.1 V, is gradually inhibited at more cathodic potentials. The current density flowing through the cell decreases and a region of cathodic passivation extends from ca. −0.15 V to the hydrogen evolution reaction (HER) potential, ca. −0.45 V. Correspondingly, during galvanostatic polarization, deposition current densities exceeding 2 mA cm^{-2} drive the potential towards more cathodic values, on average about −0.5 V, triggering the HER and causing large potential oscillations at the electrode. The current density at the onset of cathodic passivation is only slightly affected by the increase of the potential scan rate. RDE experiments confirm that the discharge of the Au(I)–TU complex occurs under non-limiting current conditions and that some kinetic hindrance interferes with the discharge reaction.

The liability of the gold surface to cathodic passivation in the acidic thiourea solution seriously impairs the plating capability of the bath. This restraint to process feasibility can be successfully overcome by adding varying amounts of halide to the solutions, preferably iodide. The addition of iodide, in the range from 1 to 30 mM, enables a substantial increase of deposition current density without detriment of deposit appearance and properties [20].

Cyclic polarization curves (0.02 V s^{-1}) between 0.07 and −0.6 V, at a stationary Au-plated Pt electrode in 1 M TU, 1 M H_2SO_4, 0.025 M Au(I), and after addition of 0.6 mM KI, are shown in Fig. 2. In the absence of iodide, the polarization curve presents a single cathodic peak at ca. −0.1 V, followed by a long tail and the onset of the HER at ca. −0.42 V. After 0.6 mM KI addition, a small anodic shift of the curve is observed along with an increase of 17% in the area of the cathodic peak at ca. −0.07 V, i.e. the electroreduction of the Au(I)–TU complex occurs with higher current efficiency. This is confirmed by the increase of the dissolution anodic current density. Figure 3 presents CP curves (0.02 V s^{-1}) between 0.1 and −0.6 V at an Au-plated Pt RDE in 1 M TU, 1 M H_2SO_4, and 0.025 M Au(I) at varying KI concentrations, 1200 rpm, and 40 °C. On increasing the iodide concentration the maximum current density at ca. −0.13 V increases and a progressive re-activation of the electrode surface is observed, as shown also by the concurrent current density increase in the anodic scan. The shape of the polarization curves changes accordingly, approaching the sigmoidal shape expected for a diffusion-controlled discharge reaction.

Low-scan LSV and CP runs were performed after addition of 0.05 M $SnSO_4$ to the base solution. Polarization curves (not shown), run at 0.001 V s^{-1} on a Pt RDE in 1 M TU, 1 M H_2SO_4, 3 mM KI, and 0.05 M $SnSO_4$ (solution A), also after addition of 0.02 M Au(I) (B), with $\omega = 1200$ rpm and at 40 °C, show a single well-defined wave starting at a potential of ca. −0.52 V in solution A; after addition of Au(I), the potentiodynamic trace shows a first wave at −0.2 V, followed by two small waves at −0.42 V and −0.48 V and, finally, at the same potential measured in the absence of Au(I), the discharge of Sn(II) ions.

The cyclic polarization behaviour is more complex. In Fig. 4 are shown CP curves run at 0.02 V s^{-1} on a stationary Pt electrode in solutions A and B. The

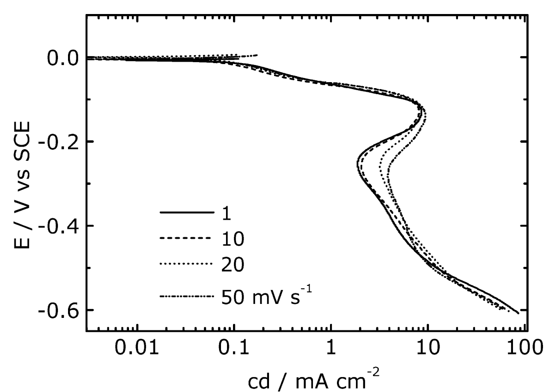

Fig. 1 Linear polarization curves at an Au-plated Pt RDE in 1 M TU, 1 M H_2SO_4, and 0.025 M Au(I) with changing potential scan rate (1200 rpm; 40 °C)

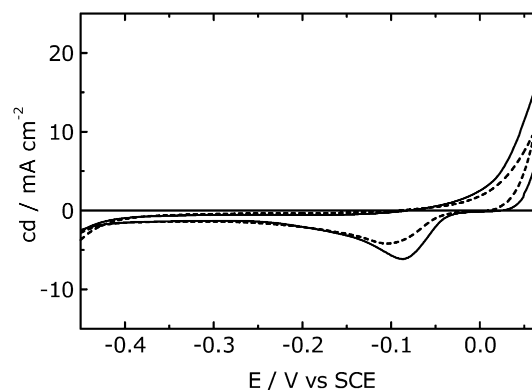

Fig. 2 CP curves (0.02 V s^{-1}) between 0.07 and −0.6 V at a stationary Au-plated Pt electrode in 1 M TU, 1 M H_2SO_4, and 0.025 M Au(I) (*dotted line*) and after addition of 0.6 mM KI (*solid line*) at 40 °C

voltammogram for solution A shows a cathodic peak for the reduction of Sn(II) and the corresponding stripping peak. In the presence of Au(I), the voltammogram, which shows only minor or no differences upon cycling, presents many new features. The cathodic peaks I–IV in Fig. 4 refer to the discharge of the Au(I)–TU complex and of Sn(II), respectively, in agreement with the potentiodynamic response. A gradually increasing current precedes peak I, starting at ca. −0.1 V. In the intermediate potential region, two other peaks appear, very close to each other and overlapping; moreover, there is a small wave at a potential of ca. −0.36 V, after which a small but sensible increase of current density results.

The anodic scan cannot be easily interpreted. Three anodic peaks partially overlapping appear in the potential range −0.55 to −0.35 V, which can be attributed to the anodic dissolution of Sn and Au-alloyed Sn deposited in the cathodic scan; the anodic peak at ca. 0 V is due to Au stripping; the increasing anodic current for potential anodic to 0.04 V is due thiourea electrooxidation at the Pt electrode [17]. In particular, none of the anodic peaks can be attributed to the oxidation of Sn(II) to Sn(IV), also because no evidence for this reaction can be seen in the CP curve in solution A.

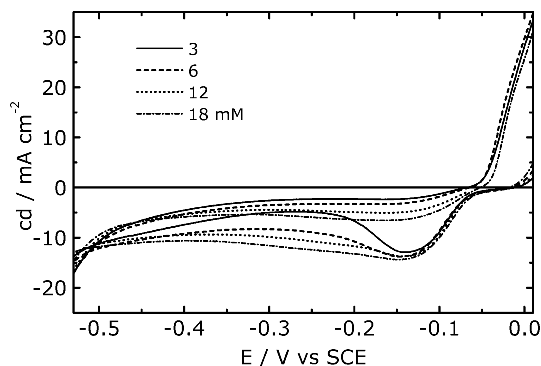

Fig. 3 CP curves (0.02 V s^{-1}) between 0.1 and −0.6 V at an Au-plated Pt RDE in 1 M TU, 1 M H_2SO_4, and 0.025 M Au(I) at varying KI concentrations (1200 rpm, 40 °C)

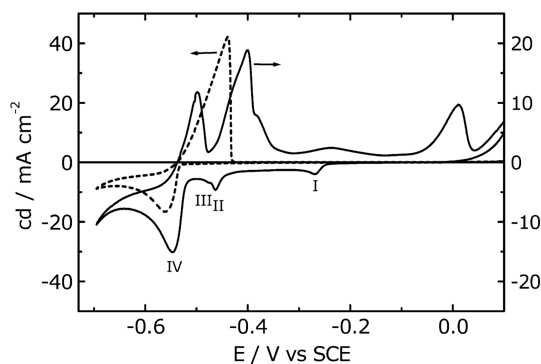

Fig. 4 CP curves at a stationary Pt electrode in 1 M TU, 1 M H_2SO_4, 3 mM KI, and 0.05 M $SnSO_4$ (*dashed line*) and the same solution + 0.02 M Au(I) (*solid line*) at 40 °C

Electrodeposition

Preliminary electrodeposition tests were carried out under DC plating. Deposits obtained in these conditions had either a single-phase structure, for a Sn content below 5 at% and in the range 8–12 at%, or a two-phase structure, consisting of the Au(Sn) terminal solution and a second phase (see below). The electrodeposition process attained reasonably stationary conditions only for a current density in a narrow range, e.g. 4–6 mA cm^{-2} with both 0.05 M Sn(II) and 0.05 M Au(I), at 40 °C on a Si/Au substrate, corresponding to the electrodeposition of Au(Sn) alloys with a face centred cubic (fcc) structure. For a given electrolyte composition, i.e. Au(I) and Sn(II) concentration, a critical current density could be identified, which marks the limit of process stability under DC plating. Above this current density value, a gradually increasing polarization causes first a progressive change in the composition of the growing layer and then destabilizes growth, resulting in powdery deposits and hydrogen evolution.

Au-Sn alloy electrodeposition was best carried out under PC plating conditions. The effect of pulse plating parameters, on-time (t_{ON}), off-time (t_{OFF}), and peak current density (i_P), on the deposit composition was studied. The Sn content in the plated alloys was mainly influenced by i_P and t_{ON}, while changing t_{OFF} in the range from 1 to 10 s did not affect appreciably the deposit composition. The effect of i_P and t_{ON} upon the Sn content in ECD alloys is shown in Fig. 5: the Sn content increases as the on-time decreases and the pulse current density increases. The change is smooth with t_{ON}, in the whole range from 0.1 to 10 s, and steep with i_P, up to 50 mA cm^{-2}. With further increase of pulse current density, the Sn content decreases abruptly. The appearance and surface morphology of the alloy coatings depend upon the composition, showing a tendency

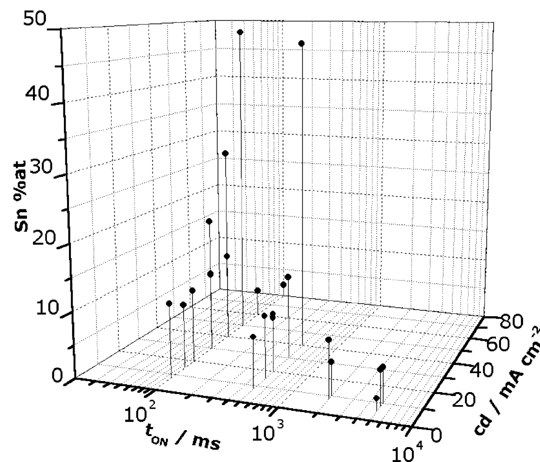

Fig. 5 Sn at% in PC electrodeposits from 1 M TU, 1 M H_2SO_4, 1.5–3 mM KI, 0.01–0.02 M Au(I), and 0.05 M $SnSO_4$, at 40 °C, on a Si/Ta/Au substrate, versus t_{ON} and peak current density

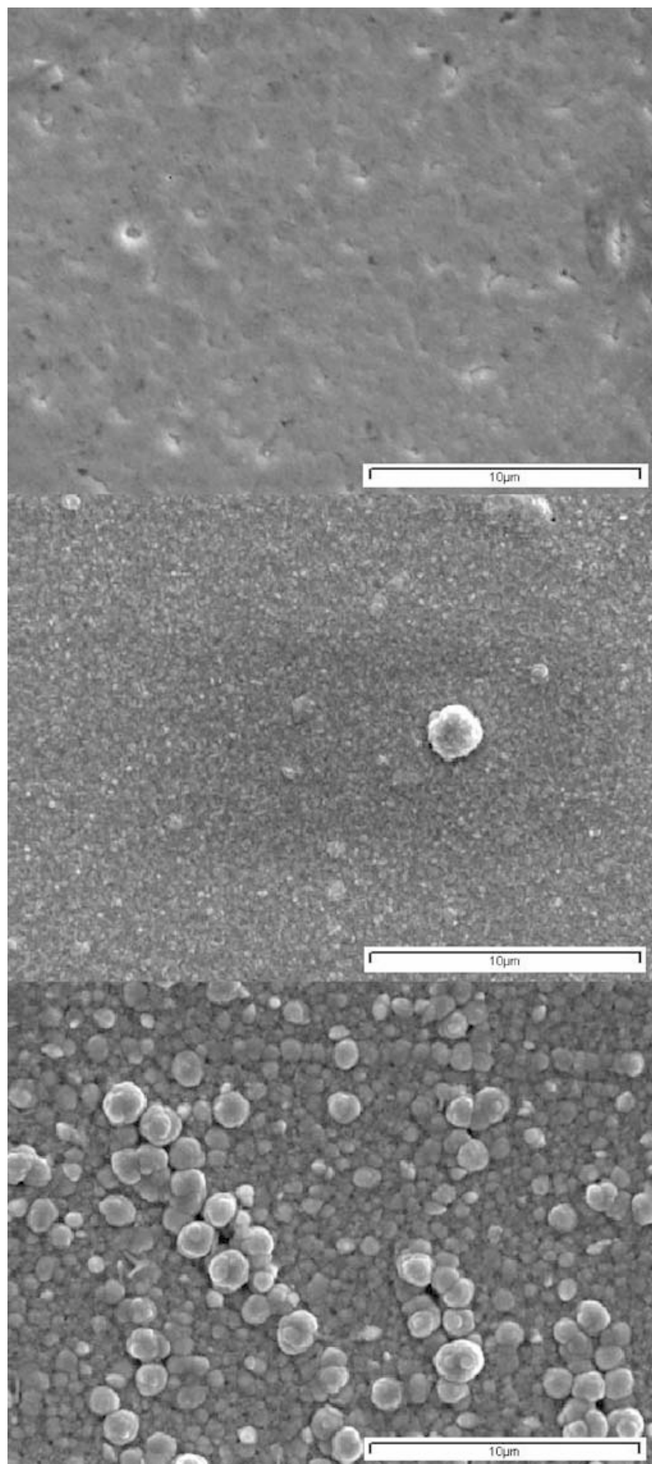

Fig. 6 *From top downwards*: surface SEM micrographs of Au-Sn with 12 at% Sn (i_P = 30 mA cm^{-2}, t_{ON} = 0.1 s, t_{OFF} = 2 s, 10^3 cycles); 30 at% Sn (i_P = 40 mA cm^{-2}, t_{ON} = 0.1 s, t_{OFF} = 2 s, 750 cycles); and 48 at% Sn (i_P = 50 mA cm^{-2}, t_{ON} = 0.1 s, t_{OFF} = 2 s, 600 cycles). Plating solution: 1 M H_2SO_4, 1 M $CS(NH_2)_2$, 0.01 M Au(I), 0.02 M Sn(II), 1.5 mM KI, 6 mM $C_6H_8O_6$; 40 °C

to become dull and coarse as the Sn content is increased. SEM micrographs of Au-Sn deposits of different composition are shown in Fig. 6.

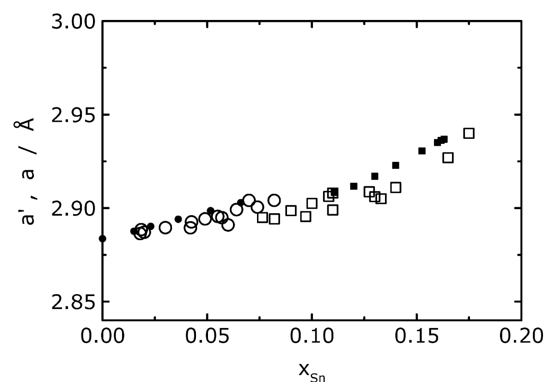

Fig. 7 Distance of closest approach in ECD (*open symbols*) and in bulk (*solid symbols*) Au-Sn alloys vs. Sn at%. Data for bulk Au-Sn alloys from Owen and Roberts [22], Nuding and Ellner [23] (α phase); Massalski and King [24], Henderson and Raynor [25] (ζ phase)

Structure and mechanical properties

In the composition range examined in this work, three different phases were identified in Au-Sn alloy electrodeposits. Alloy deposits with a Sn content up to ca. 7 at% show the fcc crystal structure of the Au-rich terminal solution of the equilibrium diagram (α phase). The maximum Sn content obtained in the electrocrystallized α phase roughly corresponds to the solubility limit of Sn in fcc Au, 6.6 at% at 532 °C [21]. For a Sn content in the range from about 9 to 18 at%, the deposit structure can be interpreted as hexagonal close packed (hcp), i.e. the same crystal structure as the equilibrium ζ phase, whose composition range extends from ca. 9.4 to 17.6 at% at 280 °C. The third phase observed in ECD alloys shows XRD patterns typical of the NiAs-type structure, which is the crystal structure of the equilibrium δ phase or the AuSn compound. However, the ECD δ phase is obtained as a single phase over a wide composition range, from about 40 to 50 at%, overcoming the stoichiometric constraint of the metallurgical phase.

ECD alloys with a Sn content in intermediate composition ranges with regard to those mentioned above have a two-phase crystal structure. This characteristic appears related to operative conditions, leading to unstable electrode polarization under direct current or triggering of the HER under pulse plating deposition.

Lattice parameter determinations confirm that the ECD phases can be identified with the equilibrium phases of the same structure type. Values of the distance of closest approach in the α and ζ phases for both ECD and bulk alloys are presented in the diagram in Fig. 7. Lattice spacings of the α phase were reported by Owen and Roberts [22] and by Nuding and Ellner [23]; those of hcp ζ Au-Sn (homogenized at 275 °C) were reported by Massalski and King [24] and Henderson and Raynor [25]. A substantial agreement is found between the values determined for the ECD fcc structure with those of the corresponding metallurgical phase; data for the ECD hcp phase are in general slightly lower than those of bulk

alloys with the same composition, possibly as a result of the strained state of the material or as a consequence of a systematic error in the lattice parameter determination. The intermediate composition range from 7 to 9 at%, where the ECD alloy structure can be either single-phase hcp or mixed fcc + hcp, corresponds in the equilibrium diagram to the stability field of the β phase and to the adjoining regions of the two-phase equilibria.

The NiAs-type structure was observed in samples with nominal composition ranging from 40 to 50 at%. When the Sn content is below about 40 at%, XRD spectra show the presence of both the ζ and δ phases. Lattice parameters of the δ phase do not show appreciable change with alloy composition: a remains almost unchanged (from 4.318 to 4.321 Å) for a Sn content varying in the range 20–50 at%; c changes from 5.515 to 5.522 Å over the same composition range. Lattice parameters for the equilibrium δ phase are: $a = 4.320$ Å and $c = 5.517$ Å (powder diffraction file JCPDS 8-463).

Microhardness and elastic modulus data, derived from indentation curves on 3 μm thick deposits on Si/Ta/Au substrates, are shown in Fig. 8. A microhardness change follows the phase structure modification: the microhardness increases linearly in the α phase field, shows a maximum of about 270 HV in the ζ phase field, and lower values in the two-phase $\zeta + \delta$ region, with only a slight increase for single-phase δ deposits. A similar change of the elastic modulus is observed for alloy deposits with the fcc structure: a linear increase up to 120 GPa for a Sn content of 7 at%, which corresponds to the solubility limit of Sn in α-Au. The elastic modulus decreases to values below 100 GPa in the ζ phase field and increases slightly in the two-phase $\zeta + \delta$ and single-phase δ regions.

Discussion

The electrochemical behaviour of acidic Au(I)–thiourea solutions is complicated by the presence of the redox couple TU/FDS and by-products of thiourea oxidation, which can interfere with the discharge reaction of the metal cations. Groenewald [17] suggested that the electroreduction of the Au(I)–TU complex and FDS could occur simultaneously on Au electrodes; Juarez and Dutra [18] showed that the Au(I) complex is actually reduced at a lower cathodic potential.

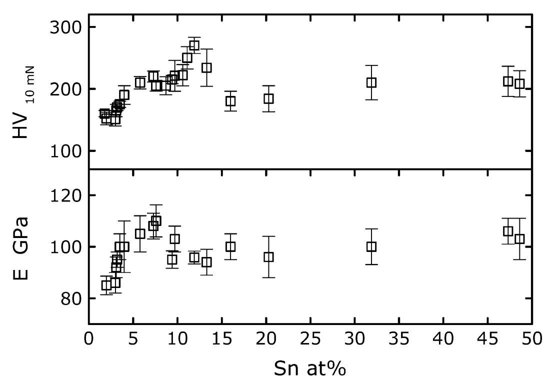

Fig. 8 HV microhardness (*top*) and elastic modulus (*bottom*) of ECD Au-Sn deposits vs. Sn content in the alloy. Data obtained by indentation depth–load measurements with a peak load of 10 mN on the surface of 3 μm thick films deposited on a Si/Ta/Au substrate

A distinctive feature of the electrochemical cathodic behaviour at an Au electrode in an acidic Au(I)–TU electrolyte is the onset of cathodic passivation at a potential of about −0.2 V (SCE) or lower. The cathodic passivation may be related either to chemisorption of thiourea oxidation products, as already suggested for Ag electrodes in thiourea solution [26], or to electroreduction of formamidine disulfide with formation of poisoning intermediates or reaction products containing sulfur, similar to the behaviour observed at a Pt electrode [27]. The effect of scan rate upon LSV curves suggests that the surface blocking is determined by poisoning adsorbates which are formed in situ during the potential scan. Increasing the potential scan rate influences the current density fall on the cathodic side of the peak, indicating that the time scale characteristic of the adsorption–passivation process is being approached. Small additions of iodide are effective in re-activating the electrode, possibly through displacement of inhibiting adsorbates and involvement in the discharge mechanism.

In the presence of Sn(II) cations in the electrolyte, CPs at a stationary Pt electrode show specific features which can be related to the formation of Au-Sn alloys at the electrode surface. The experimental evidence so far collected is still inadequate for supporting a direct correspondence between electrokinetics and structure characteristics of the ECD alloys; however, a few comments can be suggested. Cathodic polarization curves reveal the occurrence of at least three different processes in the potential range from −0.2 to −0.5 V, which could be related to the three different phases observed in ECD alloys. Besides, the closeness of peaks II and III in the CP curves (Fig. 4) provides an explanation for the structural characteristics of the alloys with composition in the range from 18 to 40 at% Sn, i.e. the formation of two-phase $\zeta + \delta$ deposits, and be significant for explaining the odd difficulty in obtaining alloy deposits with composition in the range from 30 to 40 at% Sn.

The phase structure of the ECD Au-Sn alloys obtained from acidic thiourea solutions presents significant differences from the equilibrium phase diagram, as evaluated by Okamoto and Massalski [28], also with regard to the re-examination of the Au-rich side of the diagram carried out by Ciulik and Notis [21]. The fcc terminal solution rich in Au is obtained with a Sn content up to the solubility maximum. The hcp structure corresponding to the equilibrium ζ phase is obtained in the composition range from 7 to 18 at% Sn. As the Sn content decreases from about 11 to 7 at%, the axial ratio decreases down to the value 1.633, i.e. that of an ideal hcp structure (see Fig. 9, where the axial ratio variation with composition for both ECD and metallurgical ζ phase is shown). In fact, according to the experimental evidence, the hexagonal arrangement is

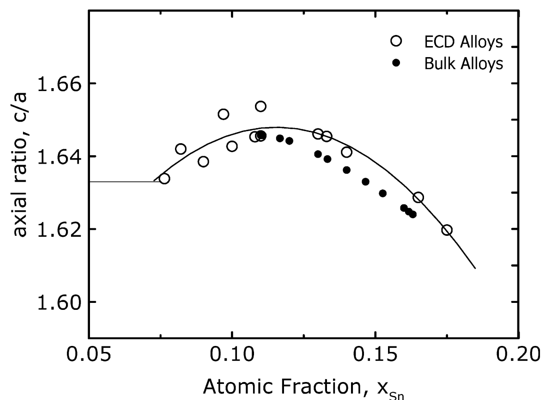

Fig. 9 Axial ratio of ECD Au-Sn alloys (*open circles*) and bulk alloys (*solid circles*) [24, 25] vs. the electron concentration (ratio of all valency electrons to the number of atoms). The *solid line* is the second-order polynomial fit of the axial ratio values for ECD alloys

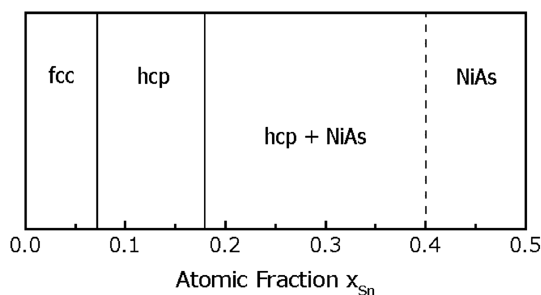

Fig. 10 Phase structure of electrodeposited Au-Sn alloys

replaced by the fcc structure, confirming that the stability limit for the ECD α phase is 7 at% Sn. Interestingly, the microhardness and axial ratio maximum occurs at similar alloy compositions. The ECD ζ phase is found to extend over a composition range close to the maximum solubility range for the equilibrium ζ phase (9.5–17.6 at% at 280 °C [1]). Contrary to its metallurgical equivalent, the ECD δ phase shows a relatively large homogeneity range, from about 40 to 50 at% Sn, whose lower boundary cannot be precisely defined, since the limits of the $\zeta+\delta$ two-phase region are ill-defined. The diagram in Fig. 10 shows the resulting composition ranges for the different phases in ECD Au-Sn alloys.

A peculiarity of the phase structure of ECD Au-Sn alloys is the practical impossibility to obtain long-range ordered structures, as we have already shown in the case of Ag-Sn and Cu-Sn alloys electrodeposited from acidic thiourea electrolytes [29]. In fact, neither the β ($TiNi_3$-type structure, $D0_{24}$) nor the ζ' phase (or Au_5Sn compound, a rhombohedral superstructure) have been identified in Au-Sn alloy deposits.

Conclusions

Au-Sn alloys with a Sn content up to 50 at% are obtained from acidic solutions containing 1 M $CS(NH_2)_2$, 1 M H_2SO_4, 0.01–0.025 M Au(I), and 0.05 M Sn(II), under PC plating conditions, with a pulse current density from 5 to 50 mA cm^{-2}, and on-time and off-time in the ranges 0.1–2 s and 1–10 s, respectively. As-deposited layers are bright or semi-bright up to 5 μm thickness, with a tendency to become dull as the Sn content is increased above about 30 at%, or also at a lower Sn content when the deposition time is increased.

In the composition range up to 7 at% Sn, ECD alloys have the fcc structure; in the composition range from about 8 to 18 at%, the alloys have the ζ phase crystal structure, with an hcp lattice and enlarged homogeneity field with respect to the equilibrium phase. Both the fcc and hcp phases are obtained over a composition range corresponding to the maximum solubility range, according to the phase diagram. The ECD δ phase, with the NiAs-type structure, is obtained over an enlarged homogeneity range. No formation of superlattice phases is observed, suggesting that, during electrochemical formation of the alloy, long-range order cannot be activated and come into play to determine the alloy phase structure, since the crystallization reactions proceed from the aggregation and local arrangement of atoms in small clusters, whose stability depends only upon interaction at the atomic and molecular scale.

Acknowledgements The authors acknowledge support from the Ministero dell'Istruzione, dell'Università e della Ricerca through MIUR 40%, project 2000, on the synthesis and characterization of Ni- and Cd-free white gold alloys.

References

1. Matijasevic GS, Lee Chin C, Wang Chen Y (1993) Thin Solid Films 223:276
2. Rapson WS, Groenewald T (1978) Gold usage. Academic Press, New York, p 235
3. Kuhn W, Zilske W (2000) US Patent 6,165,342; (1987) US Patent 4,634,505; Stevens P (1977) US Patent 4,013,523
4. Bozzini B, Giovannelli G, Natali S, Serra M, Fanigliulo A (2002) J Appl Electrochem 32:165
5. Fanigliulo A, Bozzini B, Cavallotti PL, Giovannelli G, Natali S (2002) Galvanotec Nuove Finiture 53:148
6. Sun W, Ivey DG (2001) J Mater Sci 36:757
7. Plaskin IN, Kozhukhova MA (1941) Dokl Akad Nauk SSSR 31:671
8. Kazakov VP, Lapshin AL, Peshchevitskii BL (1964) Russ J Inorg Chem 9:708
9. Gaspar V, Mejerovich AS (1994) Hydrometallurgy 34:369
10. Kirchenerova J, Purdy WC (1981) Anal Chim Acta 123:83
11. Szklarczyk M, Hoa N Nhu, Zelenay P (1996) J Electroanal Chem, 405:111
12. Bolzán A, Wakenge IB, Salvarezza RC, Arvia AJ (1999) J Electroanal Chem 475:181
13. Bolzán A, Haseeb A, Schilardi PL, Piatti RCV, Salvarezza RC, Arvia AJ (2001) J Electroanal Chem 500:533
14. Preisler P, Berger L (1946) J Am Chem Soc 69:322
15. Tataru S (1968) Rev Roum Chim 13:185
16. Groenewald T (1977) J S Afr Inst Min Metall 77:217
17. Groenewald T (1975) J Appl Electrochem 5:71
18. Juarez CM, Dutra AJB (2000) Miner Eng 13:1083
19. Lide D (ed) Handbook of chemistry and physics, 79th edn. CRC Press, Boca Raton, Fla
20. Vicenzo A, Rea M, Vonella L, Bestetti M, Cavallotti PL (2002) Galvanotec Nuove Finiture 53:209

21. Ciulik J, Notis MR (1993) J Alloys Compd 191:71
22. Owen EA, Roberts EAO'D (1945) J Inst Met 71:213
23. Nuding M, Ellner M (1997) J Alloys Compd 252:184
24. Massalski TB, King HW (1960) Acta Metall 8:677
25. Henderson B, Raynor GV (1962) Trans Faraday Soc 58:900
26. Szklarczyk M, Nhu Hoa N, Zelenay P (1996) J Electroanal Chem 405:111
27. Barber JH, Conway BE (1996) J Chem Soc Faraday Trans 92:3709
28. Okamoto H, Massalski TB (1990) Binary alloy phase diagram. ASM International, Metals Park, Ohio, pp 433–434
29. Bestetti M, Vicenzo A, Cavallotti PL (2002) In: Proc AESF SUR/FIN 2002, Orlando, Fla, pp 745–754